Int J Adv Manuf Technol (2016) 84:647–661
DOI 10.1007/s00170-015-7728-4

ORIGINAL ARTICLE

Anti-gravity gradient unique arc behavior in the longitudinal electric magnetic field hybrid tungsten inert gas arc welding

Luo Jian[1] · **Yao Zongxiang**[1] · **Xue Keliang**[1]

Received: 13 April 2015 / Accepted: 17 August 2015 / Published online: 30 August 2015

Abstract An external magnetic field applied in arc welding process results in electro-magnetic stirring (EMS) welding. The added longitudinal magnetic field (LMF) provides an effective method to control the arc behavior and affect the resultant welds. However, few studies have addressed arc behaviors in LMF-TIG hybrid welding, i.e., tungsten inert gas arc (TIG) hybrid welding with an external LMF; the LMF direction is the same as or parallel to the symmetric axis of welding arc. In this paper, a three dimensional (3D) multiphysics field model was established to analyze arc behavior in LMF-TIG hybrid welding. This model is formed by fluid dynamics equations coupled with Maxwell equations. The fields of temperature, velocity, and electric current field were obtained from this model through numerical simulation using the finite volume method (FVM). It was found that the arc changes from its free to strong electromagnetic field controlled status in three stages. After the applied electromagnetic field exceeds a critical value, mutation is induced in the arc resulting in an arc behavior completely different from that of the normal free arc. The arc pressure and temperature distributions shift their centers, where the peak pressure and temperature occur, from the tungsten axis. In addition, the arc exhibits negative pressure (i.e., anti-gravity gradient behavior) below the cathode and a tornado-style behavior. The arc plasma flow reverses, a circular area occurs, and a low-temperature zone forms in the center of the arc. The highest flow speed takes place on both sides of the arc symmetry axis. The unique appearance of the negative arc pressure and its formation mechanism are discussed.

Keywords Tungsten inert gas arc welding · Longitudinal electromagnetic field · Arc behavior · Negative pressure

✉ Luo Jian
luojian2007@gmail.com

[1] State Key Laboratory of Mechanical Transmission, College of Automotive Engineering, Chongqing University, Chongqing 400030, People's Republic of China

Nomenclature

r	Axial direction (m)
z	Radial direction (m)
T	Temperature (K)
P	Pressure (Pa)
v_r	Radial component of the speed (m/s)
v_z	Axial component of the speed (m/s)
ρ	Density of argon plasma (kg/m^3)
μ	Viscosity coefficient of argon plasma
k	Heat transfer coefficient of argon plasma (W/(m*K))
C_p	Specific heat capacity of argon plasma (J/(kg*K))
σ	Conductivity of argon plasma (S/m)
J_r	Axial component of the arc plasma current density (A/m^2)
J_z	Radial component of the arc plasma current density (A/m^2)
k_B	Boltzmann constant (J/K)
S_R	Radiative heat loss (J)
S_0	Source term of the radial momentum equations in the group of momentum equations (kg m/s)
S_Z	Source term of the axial momentum equations in the group of momentum equations (kg m/s)
φ	Potential (V)
μ_0	Vacuum permeability (T*m/A)
A_r	Radial magnetic vector potential (V*s/m)
A_z	Axial magnetic vector potential (V*s/m)
B_θ	Self-inductance magnetic field intensity (T)
R	Radius of tungsten cathode top (mm)

B_L External magnetic field intensity (T)
L Radial length of tungsten cathode side for calculating current density (mm)
θ Angle of tungsten cathode for calculating current density (°)
l Radial length on the tungsten cathode side for current distribute (mm)

1 Introduction

Electromagnetic stirring (EMS) is an effective method to control the solidification in metals with extensive practical backgrounds and solid industrial bases. In recent years, its studies and applications have been on the rise. In particular, an external longitudinal magnetic field, also known as coaxial magnetic field [1], can promote the rotation of arc and change the radial distribution of the plasma jet and that of the current density. These changes affect the heating and melting of the base metal as well as the formation of the resultant welds. Specifically, electromagnetic stirring in arc welding is found to refine the primary solidification structure of the welded metal, reduce the chemical inhomogeneity, enhance the ductility and toughness of the material, and improve the weld quality [2]. Further, the added electromagnetic field can determine the properties of the resultant welds and welded structure directly [3].

Due to the high temperature, electromagnetic radiation, and arc conditions in TIG, direct measurements for arc properties (including temperature field, arc plasma pressure, and velocity field) have been challenging [4–7]. Therefore, numerical simulation methods have been extensively used to study the arc plasmas behavior, welding pool behavior, and microstructure and so on [8–13]. The welding heat transfer is currently considered preferred in these cases [6–8]. Within past decades, welding arc behaviors have been extensively studied via simulation with or without external magnetic field [14–18]. Hsu et al. [19] used magnetic fluid dynamics (MHD) equations to simulate conventional arc behavior in the TIG welding environment and analyzed the temperature field of an arc by applying the spectroscopy experimental method. Wu et al. [20] established a numerical model for TIG to obtain the temperature field, velocity field, and current density field of the welding arc. Their models utilized the magnetic induction vector method to calculate the strength of the self-inductance magnetic field through integration, and the simulation results were in good agreement with experimental ones. Li et al. [21, 22] used the FLUENT computational fluid software to establish an arc model with an external magnetic field applied and obtained the temperature field and velocity field of the arc. The results showed that the applied external magnetic field can increase the tangential velocity of electric-charged particles in the arc plasmas and cause the arc's shape expand. Yu et al. [23] used a two-dimensional (2D) axisymmetric model to study the arc with a constraint welding nozzle to obtain the velocity, temperature, current density, and electromagnetic force field about the constrained arc. They found that the pressure distribution mainly depends on the current and inlet pressure rather than the arc length. Takehiko et al. [24] utilized MHD theory and related equations, which were solved by the FVM, to investigate the welding current impact, cathode diameter, and argon flow rate on the DC arc shape under an AC magnetic field. The simulation accuracy was validated by comparing computational and experimental results. Wang et al. [25] established a vacuum arc model under the force of an external magnetic field based on the MHD theory. Temperature and current density fields were obtained for vacuum arcs. It was found that that the restriction effect, the applied magnetic field generated to the vacuum arc, is mainly due to the Hall effect.

Unfortunately, few studies have been done on the simulation to study the arc behaviors in LMF-TIG hybrid welding, especially for threshold conditions from conventional free arc to the expected constraint arc [4, 7]. In this paper, MHD equations with the electromagnetic induction vector were applied, including the mass continuity equation, energy equation, Ohmic equations, and Maxwell equations. Partial differential equations were solved to obtain the self-inductance magnetic field. The Maxwell equations are coupled to the hydrodynamic equations. The Lorentz force, Joule heating, and radiant heat loss were added to the momentum equation and energy equation as source terms. The temperature, velocity, current density, and magnetic field were obtained. With the computed fields, the effects of the added external LMF and the welding current on the TIG welding arc were also studied. A theoretical foundation is thus provided to guide possible industrial applications of the LMF-TIG hybrid welding.

2 Model

The model for the arc in LMF-TIG hybrid welding is illustrated in Fig. 1. Charged particles in the arc plasmas rotate around the symmetry axis of the arc under the Lorentz force generated by the self-inductance magnetic field. When an external electromagnetic field is present, a series of complex and profound changes occur in arc behaviors and properties, including its temperature, velocity, and electric field as well as the arc shape. These distinctive changes in the arc come from the motion of charged particles in arc plasmas. This is a result of the Lorentz force generated by the applied external LMF. In

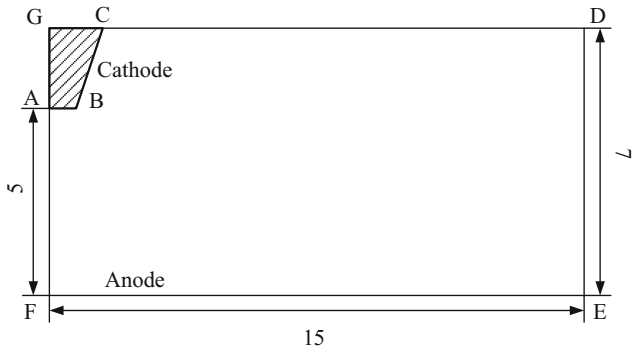

Fig. 1 Geometric model of LMF-TIG hybrid welding arc

this paper, the LMF is assumed to be a uniform and stable electromagnetic field, i.e., with a constant strength but a downward direction.

2.1 Fundamental assumptions

Based on the characteristics of LMF-TIG hybrid welding arc [26–31], the following assumptions are made:

1. The arc is axisymmetric and the gas shield environment is the incompressible pure argon which fills the entire space of interest.
2. The arc plasma flow is laminar.
3. The arc plasma satisfies the local thermodynamic equilibrium (LTE) condition.
4. The arc plasma is optical thin film.
5. Physical properties, including density, specific heat capacity, heat transfer coefficient, conductivity, viscosity of the arc plasma, are only temperature dependent.
6. The gravity and viscous occurred thermal diffusion are negligible.

2.2 Governing equations

The governing equations describing movement characteristics of the LMF-TIG hybrid welding arc are as follows under the stable or axisymmetric conditions:

1. Continuity equation

$$\frac{1}{r}\frac{\partial(\rho v_r)}{\partial r}+\frac{\partial(\rho v_z)}{\partial z}=0 \tag{1}$$

2. Radial momentum equation

$$\frac{1}{r}\frac{\partial\left(r\rho V_r^2\right)}{\partial r}+\frac{\partial(\rho V_z V_r)}{\partial z}=-\frac{\partial P}{\partial r}+\frac{1}{r}\frac{\partial}{\partial r}\left(2r\mu\frac{\partial V_r}{\partial r}\right)+\frac{\partial}{\partial z}\left[\mu\left(\frac{\partial V_z}{\partial r}+\frac{\partial V_r}{\partial z}\right)\right]-2\mu\frac{V_r}{r^2}+S_0 \tag{2}$$

3. Axial momentum equation

$$\frac{1}{r}\frac{\partial(r\rho V_r V_z)}{\partial r}+\frac{\partial\left(\rho V_z^2\right)}{\partial z}=-\frac{\partial P}{\partial z}+\frac{\partial}{\partial z}\left(2\mu\frac{\partial V_z}{\partial z}\right)+\frac{1}{r}\frac{\partial}{\partial r}\left[r\mu\left(\frac{\partial V_z}{\partial r}+\frac{\partial V_r}{\partial z}\right)\right]+S_z \tag{3}$$

4. Energy equation

$$\frac{1}{r}\frac{\partial}{\partial r}\left(r\rho C_p V_r T\right)+\frac{\partial}{\partial z}\left(\rho C_p V_z T\right)=-\frac{1}{r}\frac{\partial}{\partial r}\left(rk\frac{\partial T}{\partial r}\right)+\frac{\partial}{\partial z}\left(k\frac{\partial T}{\partial z}\right)+\frac{J_r^2+J_z^2}{\sigma}+\frac{5K_B}{2e}\left(J_r\frac{\partial T}{\partial r}+J_z\frac{\partial T}{\partial z}\right)-S_R \tag{4}$$

Where J_r and J_z are obtained by solving the Maxwell equations based on the electromagnetic induction vector method.

5. Current continuity equation

$$\frac{1}{r}\frac{\partial}{\partial r}\left(r\sigma\frac{\partial\varphi}{\partial r}\right)+\frac{\partial}{\partial z}\left(\sigma\frac{\partial\varphi}{\partial z}\right)=0 \tag{5}$$

6. Ampere's law

$$\frac{1}{r}\frac{\partial}{\partial r}\left(r\frac{\partial A_z}{\partial r}\right)+\frac{\partial}{\partial z}\left(\frac{\partial A_z}{\partial z}\right)=-\mu_0 J_z \tag{6}$$

$$\frac{1}{r}\frac{\partial}{\partial r}\left(r\frac{\partial A_r}{\partial r}\right)+\frac{\partial}{\partial z}\left(\frac{\partial A_r}{\partial z}\right)=-\mu_0 J_r \tag{7}$$

7. Ohm's law

$$J_z=-\frac{\partial\varphi}{\partial z} \tag{8}$$

$$J_r=-\frac{\partial\varphi}{\partial r} \tag{9}$$

Where the vacuum permeability $\mu_0=-4\pi\times 107$ T·m/A.

8. Self-inductance magnetic field

From the Eqs. (6) and (7), the strength of the self-inductance magnetic field B_θ can be expressed as follows:

$$B_\theta=\frac{\partial A_z}{\partial r}-\frac{\partial A_r}{\partial z} \tag{10}$$

In this paper, the SIMPLE algorithm was used to solve the MHD and Maxwell's coupled equations. The last three terms in the energy Eq. (4) are the Joule heating, electronic thermal, and radiation heat loss, respectively. They are added to the energy Eq. (4) as the source term.

2.3 Geometric model and boundary conditions

The following geometric model is adopted in this study: ABCG represents the tungsten cathode in the TIG welding; the cone angle of the cathode is 60°; EF is the metal plate anode; the arc length is 5 mm, which is the vertical distance AF. ABCDEF is the computing area of arc space, which is also the flow area and electromagnetic area. The shield gas is assumed to be pure argon, its properties including density, viscosity, heat transfer coefficient, and conductivity below the temperature of 30,000 K are given in ref. [7], which are recognized and widely cited by many researchers. The welding current is used from 100 to 300 A. The strength of the LMF used ranges from 0 to 0.03 T.

The electric potential of EF is 0. The inlet velocity of CD is 5 m/s with the initial temperature set at 1000 K. DE is the outlet and the initial temperature is also 1000 K. The inlet CD and outlet DE are both under a boundary condition of one standard atmospheric pressure. The current density is loaded on the surface of tungsten cathode, i.e., AB and BC, and the maximum current density $J_{\max}$ and current density $J(l)$ satisfy the following conditions:

$$I = \int_0^R 2\pi r J_{\max} dr + \int_0^L 2\pi (R + l\sin\theta) J(l) dl \tag{11}$$

$$J(l) = J_{\max}\left(1 - \frac{l}{L}\right) \tag{12}$$

Where θ is 30° and L is 0.4 mm.

The boundary conditions are shown in Table 1.

3 Results and discussion

The temperature, velocity, current density, electromagnetic, and pressure field of arc plasmas are obtained in the LMF-TIG hybrid welding by the FVM numerical simulation.

3.1 Temperature fields

Figures 2 and 3 show the temperature field for LMF-TIG hybrid welding arc when the welding current is 200 and 300 A, respectively.

Based on the isotherm shape of TIG welding arc, the conventional free welding arc without a LMF applied exhibits a typical solid bell shape. The highest temperature appears below the cathode vertically. The temperature increases with the increase of the welding current. The maximum of temperature is 20,000 K when the welding current is 200 A, and it rises to 25,000 K when the welding current is 300 A, which are shown in the Figs. 2a and 3a.

When the LMF is applied, the welding arc shape changes significantly: The upper part of the arc (near the cathode) contracts, while the bottom part (near the anode) expands axially, leading to a hollow bell shaped arc (shown in the Figs. 2b, c and 3b, c). When the strength of the LMF increases exceeding a certain value, the variation of arc isotherm shape is more obvious: the isotherms (close to the anode) on the symmetry axis offset upward (to cathode direction) and result in a lower temperature area appearing beneath the cathode (near the anode).

At the same time, the peak temperature shows a certain degree of rise with the increase in the strength of LMF. The highest temperature is about 21,000 K for a 200-A welding current and a 0.03-T magnetic induction strength in Fig. 2d, 26,000 K for a 300 A welding current and a 0.02-T magnetic field in Fig. 3c, 27,000 K for a 300-A welding current and a 0.03-T magnetic field in Fig. 3d, respectively.

3.2 Flow fields

Figures 4 and 5 show velocity contours when the welding current is 200 and 300 A, respectively.

When welding current is 200 A without the LMF, the highest speed of the welding arc plasmas is 140 m/s, which occurs directly below the cathode and is of a downward

Table 1 The boundary conditions of LMF-TIG hybrid welding arc

Name	AB	BC	CD	DE	EF	FA
P			1.013×10^5 Pa	1.013×10^5 Pa		$\frac{\partial\Omega}{\partial n}=0$
T	3000 K	3000 K	1000 K	1000 K	1000 K	$\frac{\partial\Omega}{\partial n}=0$
φ	$J_{\max}$	$J(l)$	$\frac{\partial\Omega}{\partial n}=0$	$\frac{\partial\Omega}{\partial n}=0$	$\frac{\partial\Omega}{\partial n}=0$	$\frac{\partial\Omega}{\partial n}=0$
A_i	$\frac{\partial\Omega}{\partial n}=0$	$\frac{\partial\Omega}{\partial n}=0$	$\frac{\partial\Omega}{\partial n}=0$	$\frac{\partial\Omega}{\partial n}=0$	0	$\frac{\partial\Omega}{\partial n}=0$
v			5 m/s			$\frac{\partial\Omega}{\partial n}=0$

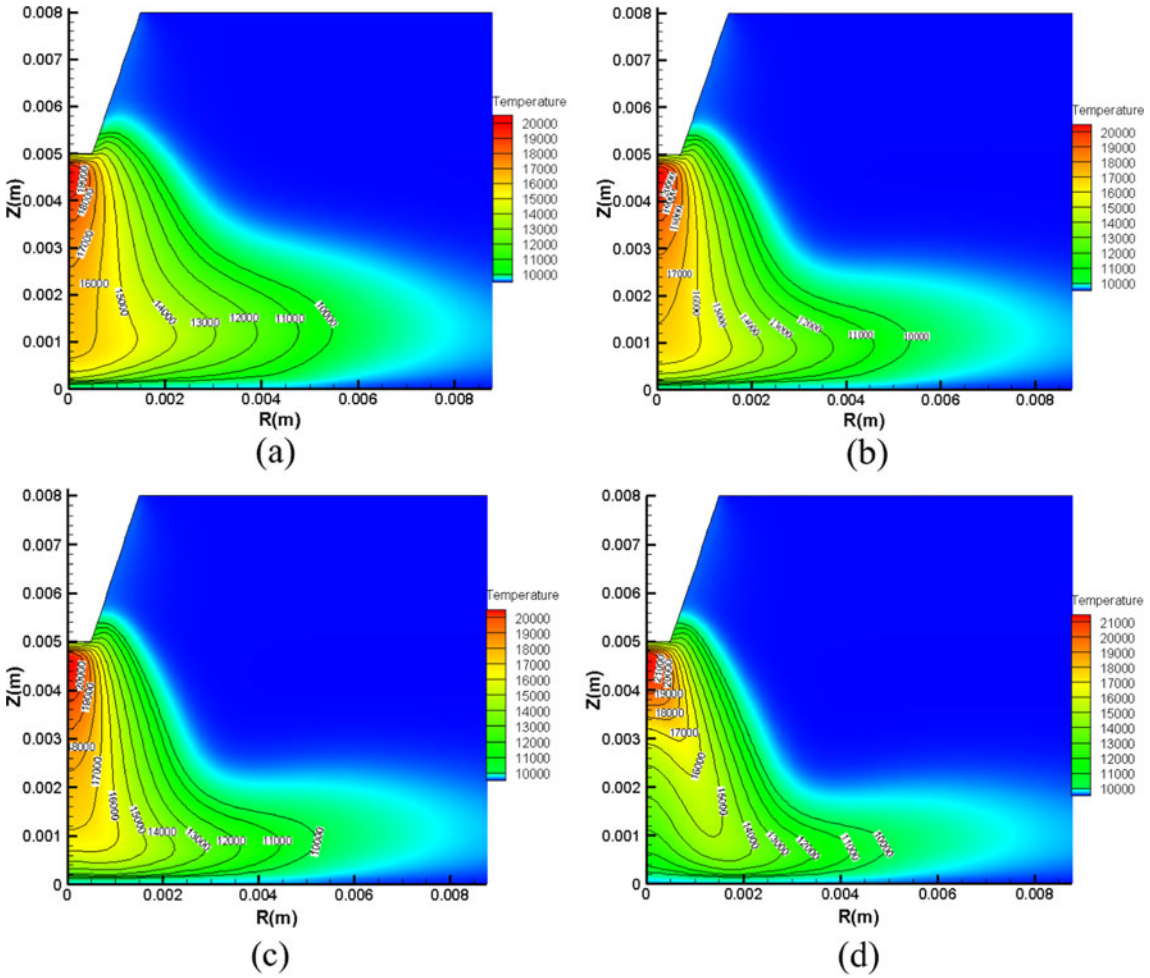

Fig. 2 Temperature fields of LMF-TIG hybrid welding arc when welding current is 200 A with a different magnetic induction strength: **a** B_L=0, **b** B_L= 0.01 T, **c** B_L=0.02 T, **d** B_L=0.03 T

direction as can be seen in Fig. 4a. When the magnetic induction strength is 0.01 T, the velocity field of welding arc has obvious expansion (Fig. 4b). The highest velocity of welding arc also locates directly below the cathode and is of downward direction, but the value reduces to 130 m/s. When the magnetic induction strength is 0.02 T, the highest speed basically stays unchanged but has a declining tendency (Fig. 4c). The maximum velocity changes to occur on the right rather than directly below the cathode, and the speed direction is still downward.

When the magnetic field strength is 0.03 T, a remarkable change occurs in the velocity field of welding arc as can be seen in Fig. 4d. The velocity distribution is of two different characteristic regions. A clear circumfluence appears below the cathode and is close to the anode. The highest velocity area locates at the two sides of center symmetry axis and near the cathode. The charged particles move in a clockwise direction in the loop zone, i.e., the movement direction is vertical from anode to cathode in the symmetry axis. The peak of the velocity field is 130 m/s, which appears at the both sides of symmetry axis and near the cathode.

When the welding current is 300 A without a LMF, the maximum speed of the free welding arc is 360 m/s, which occurs below the cathode, and has a downward direction (Fig. 5a). When the LMF is 0.01 T, the velocity field also exhibits an obvious expansion. The highest velocity also occurs under the cathode, but the value reduces to 320 m/s. When the LMF is 0.02 T, the maximum speed still locates under the cathode but reduces to 300 m/s as can be seen in Fig. 5c. When the LMF is 0.03 T, the velocity distribution similarly has two different characteristic regions (Fig. 5d). The clear circumfluence area also appears near the anode and locates below the cathode. The highest velocity area also transfers into the two sides of the symmetry axis. In the loop zone, the charged particles move in the clockwise direction and flow vertically from anode to cathode. The highest speed is 260 m/s, which happens at the both sides of the cathode.

3.3 Pressure fields

Figure 6 shows the pressure fields when the LMF is 0.03 T with 200- and 300-A welding current. The minimum pressure

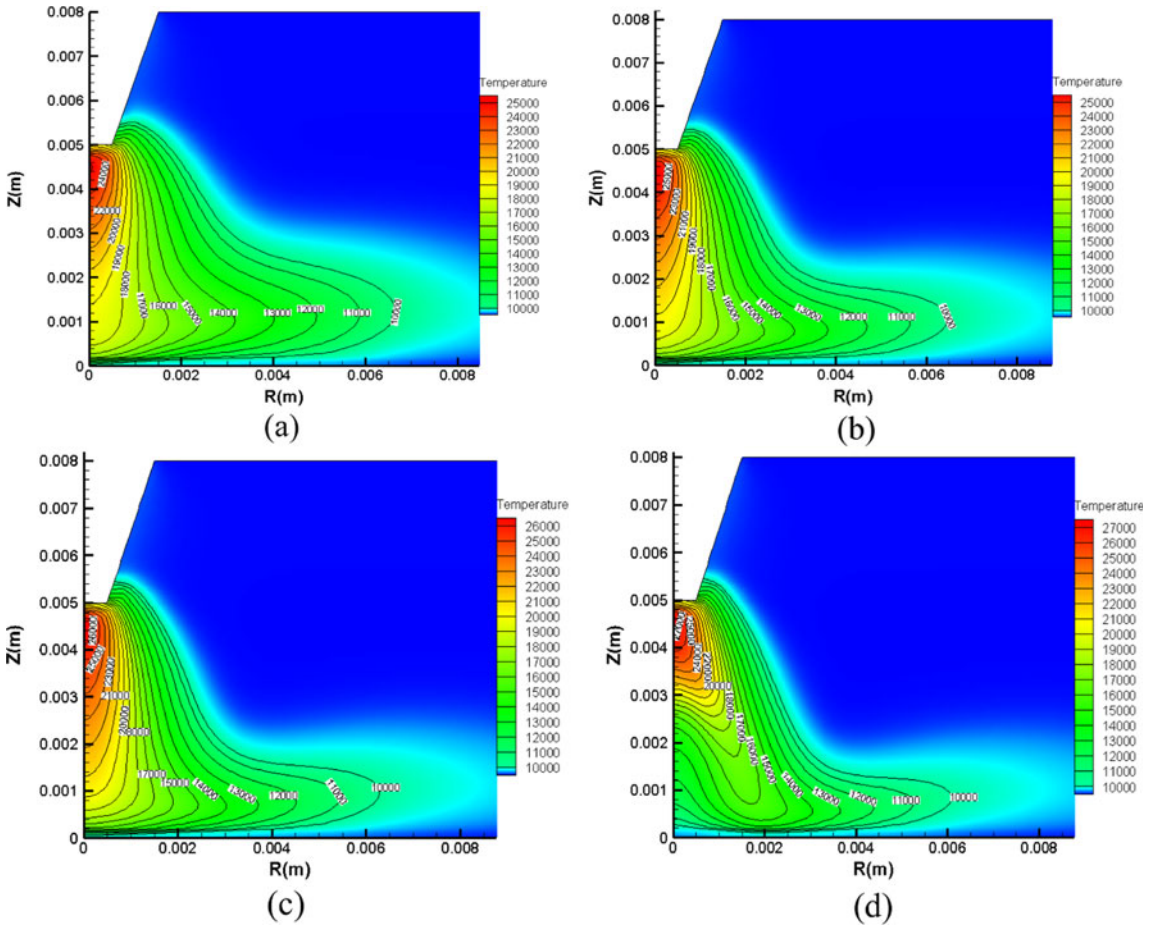

Fig. 3 Temperature fields of LMF-TIG hybrid welding arc when welding current is 300 A with a different magnetic induction strength: **a** B_L=0, **b** B_L= 0.01 T, **c** B_L=0.02 T, **d** B_L=0.03 T

of the welding arc occurs below the cathode. Higher pressures achieve at the locations closer to the anode along the symmetry axis (Fig. 6a) or farther away from the arc center along the radial direction. The maximum pressure occurs close to the surface of the anode where the R is 0.002 m (Fig. 6b). Because the welding arc is driven to rotate by the Lorentz force from the LMF, the charged particles are spiral downward under this effect. When the particles reach the anode, a circumfluence area with an about 1.5-mm radial scale appears. This is a new unique characteristic about the pressure distribution in the LMF-TIG hybrid welding.

Combined with analysis of radial velocity, the pressure distribution characteristic of welding arc is confirmed, and the radial velocity field of welding arc also helps to better understand the pressure distribution. The radial speed distributions with a 200-A welding current are shown in Fig. 7.

Under the conventional TIG welding conditions, the maximum radial velocity of the free arc is 30 m/s, where it locates near the anode area (Fig. 7a). After applying the LMF, the maximum radial velocity of welding arc increases with the increase of the magnetic field strength (Fig. 7b–d). However, the radial velocity of the particles reduced from 40 to 30 m/s (Fig. 7d) in the upper part of the arc (close to the cathode). When the LMF is 0.03 T, the radial velocity of the arc particle is negative near the circumfluence zone; namely, the charged particles move from the edge of the arc to the arc center, which coincides with Figs. 4d and 5d. The radial speed field of LMF-TIG hybrid welding arc is in agreement with the pressure field's results.

3.4 Evolution process of welding arc

The above result and analysis indicate that the applied LMF has significant influences on the temperature, speed, pressure, and energy distribution of the welding arc. The influence varies with the LMF strength, as shown in Figs. 4 and 5. Therefore, it is necessary to study the evolution process of the welding arc under LMF effect in order to provide a new principle for welding arc and promote LMF industrial application.

Because LMF typically used in welding engineering application is relatively small, a 200-A welding current with a LMF less than 0.03 T was used in this study. Figure 8 shows the

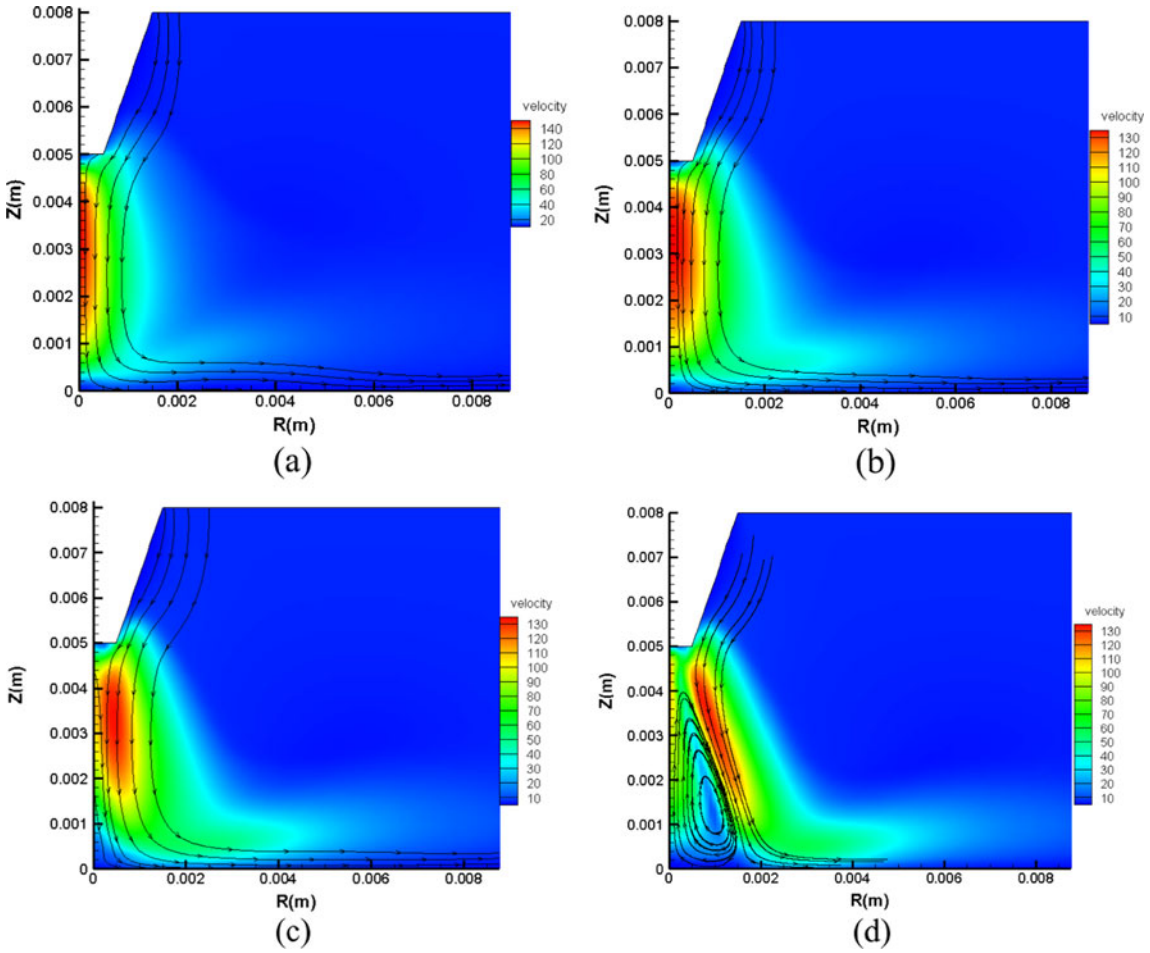

Fig. 4 Velocity field of LMF-TIG hybrid welding arc when welding current is 200 A with a different magnetic induction strength: **a** B_L=0, **b** B_L=0.01 T, **c** B_L=0.02 T, **d** B_L=0.03 T

evolution process of the TIG welding arc with the increase of the LMF under a constant welding current of 200 A.

In Fig. 8, the arc begins to expand with the strength increase in the LMF. When the induction intensity raises exceeding a certain critical value or threshold, a low-temperature area occurs near the anode under the cathode of the welding arc. This can be ascribed to effects of the Lorentz force from the applied longitudinal electromagnetic field.

For example, on the center symmetry axis (oz), the z coordinate of 17,000 K isotherm of welding arc is 0.0026 m without the LMF (Fig. 8a), 0.0015 m when the LMF is 0.01 T (Fig. 8b), and 0.0012 m when the LMF is 0.015 T; the welding arc still expands as can be seen in Fig. 8c. However, when LMF is 0.018 T (Fig. 8d), there is no obvious change on the z direction coordinate, and the welding arc shape is similar to that when the LMF is 0.015 T. In other words, the region of 17,000 K isotherm of welding arc reduces gradually on the LMF-TIG hybrid welding process.

When the LMF reaches 0.02 T (Fig. 8e) and 0.022 T (Fig. 8f), the coordinate of the 17,000 K isotherm of welding arc stays unchanged on the center symmetry axis (oz). However, the 16,000 K isotherm warps slightly upward. At the same time, charged particles in the welding arc at the anode area (near the symmetry axis) expand continuously under the effect of LMF. A low-temperature area starts to happen but there has still no circumfluence. As the magnetic field strength increases reaching 0.024 T, z coordinate of 17,000 K isotherm is 0.0014 m and the isotherm warps slightly upward (Fig. 8g). Until now, a clear low-temperature area appears and the welding arc also exhibits an axial shrinkage. At this time, a small circumfluence area appears at the symmetry axis (near the anode), and pressure field also changes owing to the Lorentz force from the LMF (see Fig. 6). With the LMF strength increase, from Fig. 8h–j, the z coordinate of 17,000 K isotherm increases to 0.0027 m, and the loop area of welding arc temperature enlarges. The welding arc shape has no obvious variation but the low-temperature area of welding arc appears more clear at the symmetry axis, where it is beneath the cathode near the anode.

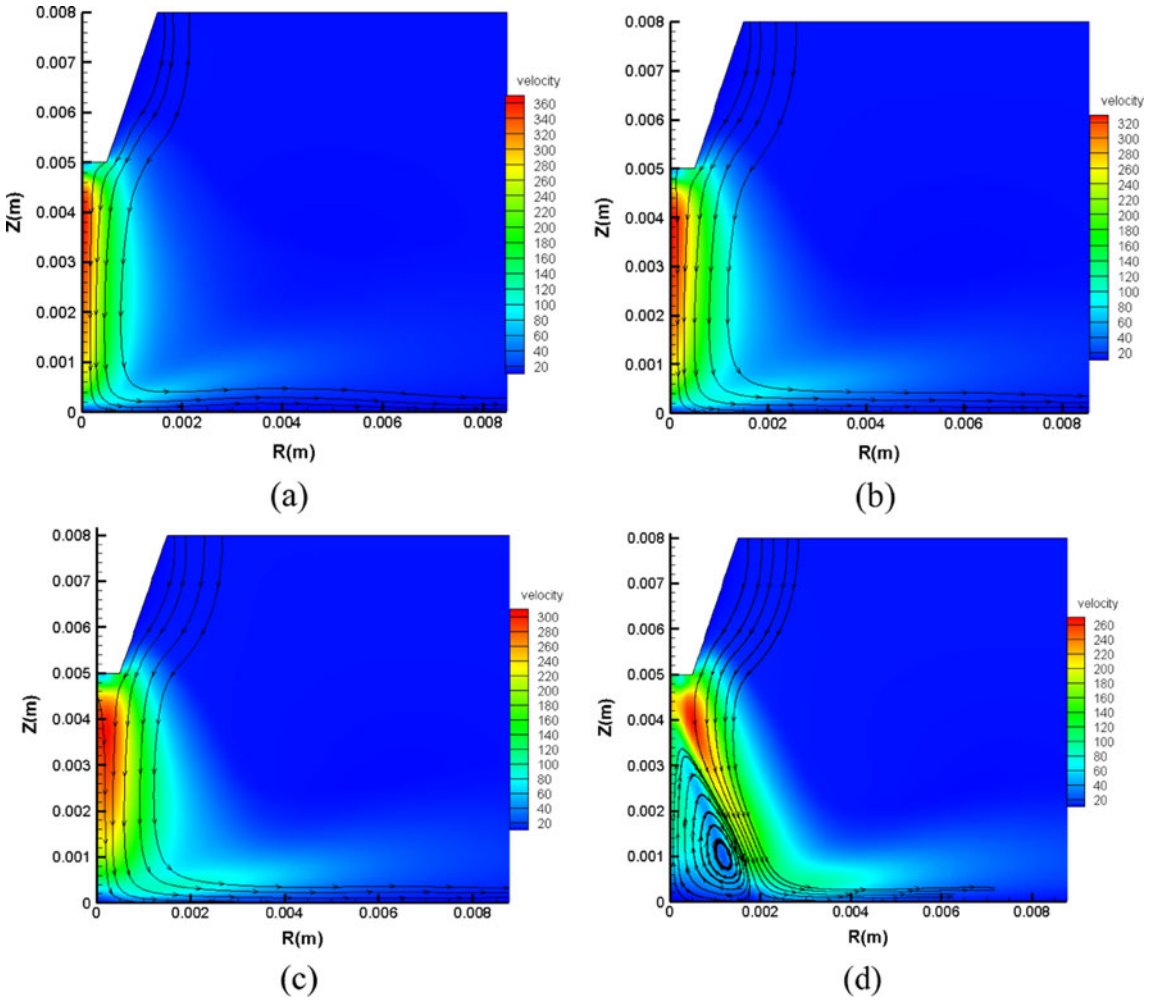

Fig. 5 Velocity field of LMF-TIG hybrid welding arc when welding current is 300 A with a different magnetic induction strength: **a** B_L=0, **b** B_L=0.01 T, **c** B_L=0.02 T, **d** B_L=0.03 T

In summary, the TIG welding arc expands under the effect of the LMF. When the LMF strength increases to a certain value, the TIG welding arc will experience the axial contraction and a low-temperature area may appear

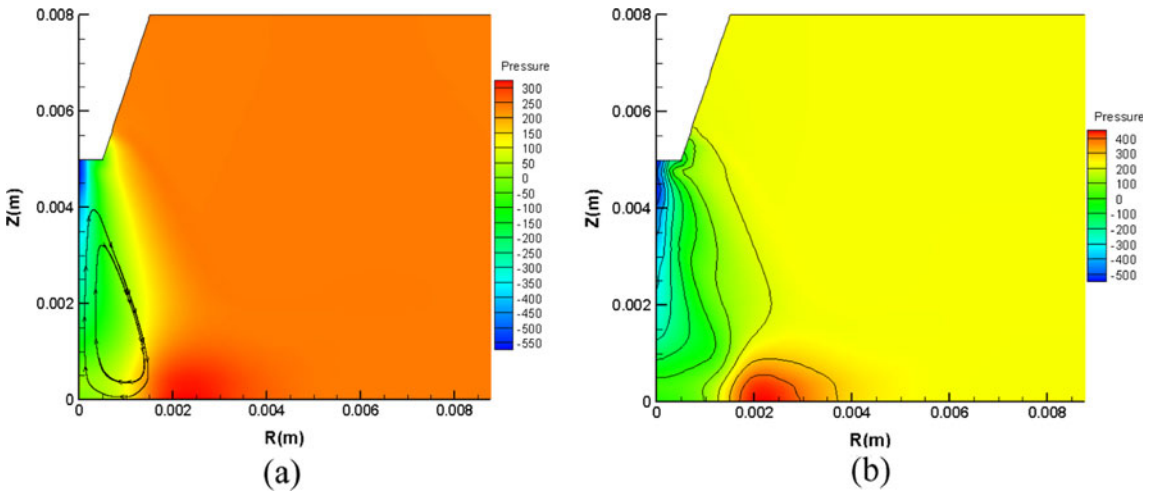

Fig. 6 Pressure field of the LMF-TIG hybrid welding arc when magnetic induction strength is 0.03 T with a different welding current: **a** 200 A, **b** 300 A

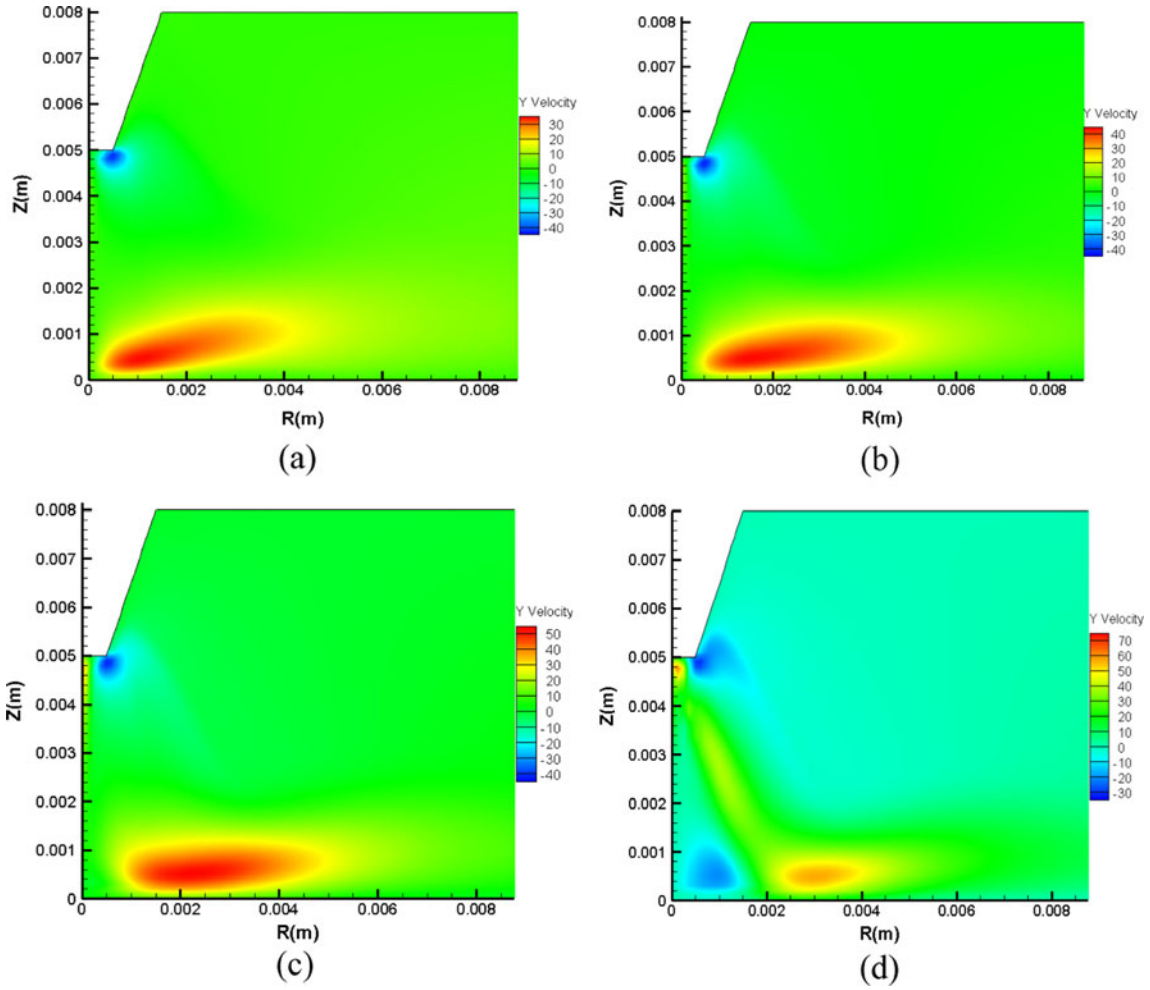

Fig. 7 Radial velocity field of LMF-TIG hybrid welding arc when welding current is 200 A with different magnetic induction strengths: **a** B_L=0, **b** B_L=0.01 T, **c** B_L=0.02 T, **d** B_L=0.03 T

under the cathode near the anode. Meanwhile, a circumfluence zone of heat flow will generate and form in the low-temperature area of welding arc.

However, it is necessary to determine the critical value of the LMF, at which the significant changes (such as the formation of the circumfluence and low-temperature area) start to take place. In order to illustrate this change, the axial variation of the 17,000 K isotherm was taken as an evaluation standard. It is assumed that strengths of the LMF are B_i, B_{i+1}, and B_{i-1}, and the corresponding axial coordinates of the 17,000 K isotherm are Z_i, Z_{i+1}, and Z_{i-1}. It is believed that the strength of the LMF is the critical value B_i when the ratio φ meets

$$\varphi = \frac{Z_{i+1} - Z_i}{Z_i - Z_{i-1}} < 0 \quad \text{and} \quad |\varphi| \leq 1 \tag{13}$$

The properties of the welding arc, including the shape, heat flow, pressure, and velocity, would obviously change when the critical LMF is applied in the TIG welding process. In this case, the critical value of the LMF is 0.022 T with a 200-A welding current.

3.5 Movement mechanism

The shield gas flows in parallel with the direction from the cathode to anode at a relatively high speed. The temperature of welding arc at the center is higher. As a result, the particles also move from the center to the side in the welding arc column. On the other hand, the temperature of arc in the anode is lower than that in the cathode, and the shape size of arc in the cathode is larger than that in the anode. Thus, the axial movement direction of welding arc plasmas is from cathode to anode. The flow paths are not straight lines but curved. In fact, the movement orbit of particles is spiral, which makes up for a series of helical bundle around the symmetry axis of welding arc. These above analyses are shown in Fig. 9.

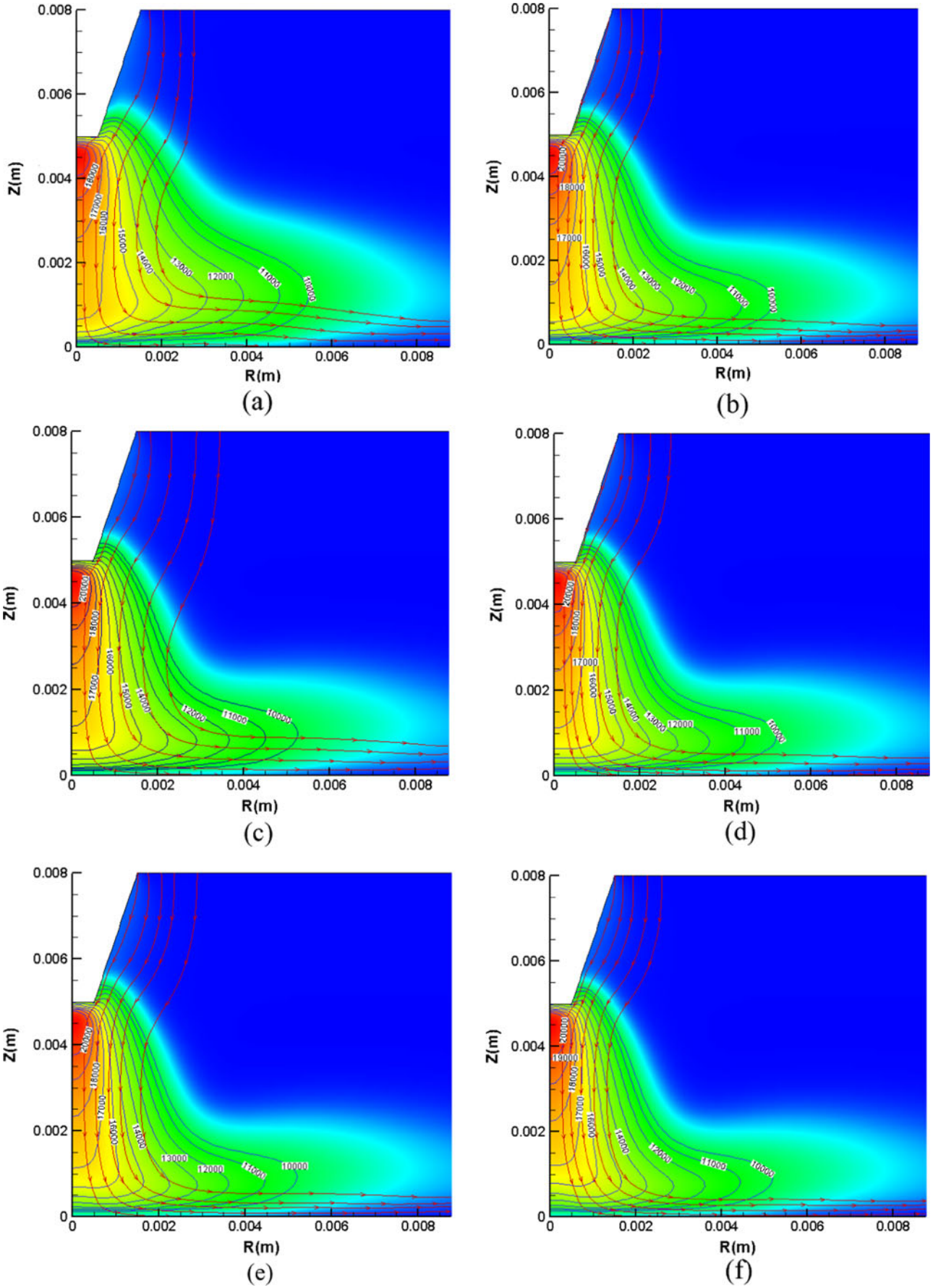
Z(m)
R(m)
0.008
0.006
0.004
0.002
0
0.002
0.004
0.006
0.008
(a)
(b)
(c)
(d)
(e)
(f)

◀ **Fig. 8** Evolution process of LMF-TIG hybrid welding arc when welding current is 200 A with different magnetic induction strengths: **a** B_L=0, **b** B_L=0.01 T, **c** B_L=0.015 T, **d** B_L=0.018 T, **e** B_L=0.02 T, **f** B_L=0.022 T, **g** B_L=0.024 T, **h** B_L=0.026 T, **i** B_L=0.028 T, **j** B_L=0.03 T

In this case, a constant welding current is applied. The charged particles of the free welding arc have a certain spiral radius around the symmetry axis owing to these influences from the self-inductance magnetic field and temperature field. When the LMF is applied, additional Lorentz force is generated on these particles, which originated from the LMF with a radial velocity component (V_1 and V_2 in Fig. 9). These particles in the welding arc will rebalance and reach a re-equilibrium state as a result of these above factors: self-inductance magnetic field, LMF, and temperature field. Meanwhile, these particles make the same spiral motion around the symmetry axis of the welding arc. Due to the Lorentz force from the LMF, the movement of particles is changed, leading to consequent changes in the velocity, current density, plasmas pressure, and temperature field in the LMF-TIG hybrid welding.

As shown in Fig. 9, the radial velocity component of particles has the opposite direction at the arc's upper part and bottom part. The particles at the upper part move from the arc edge to the arc center, while those at the lower part of the arc transport from the center to the edge. The Lorentz forces on charged particles at the upper and lower are also completely opposite under the effect of the LMF. And there has a large radial temperature gradient from the arc center to the arc edge, so the radial velocity of particles at the upper part of welding arc is restrained by the driving force from the temperature gradient, while those at the lower part of welding arc is amplified (shown in Fig. 7). When the LMF is less than the critical electromagnetic induction intensity, the particles spiral around the symmetry axis; these particles are in equilibrium. However, the higher the speed of the particle, the larger

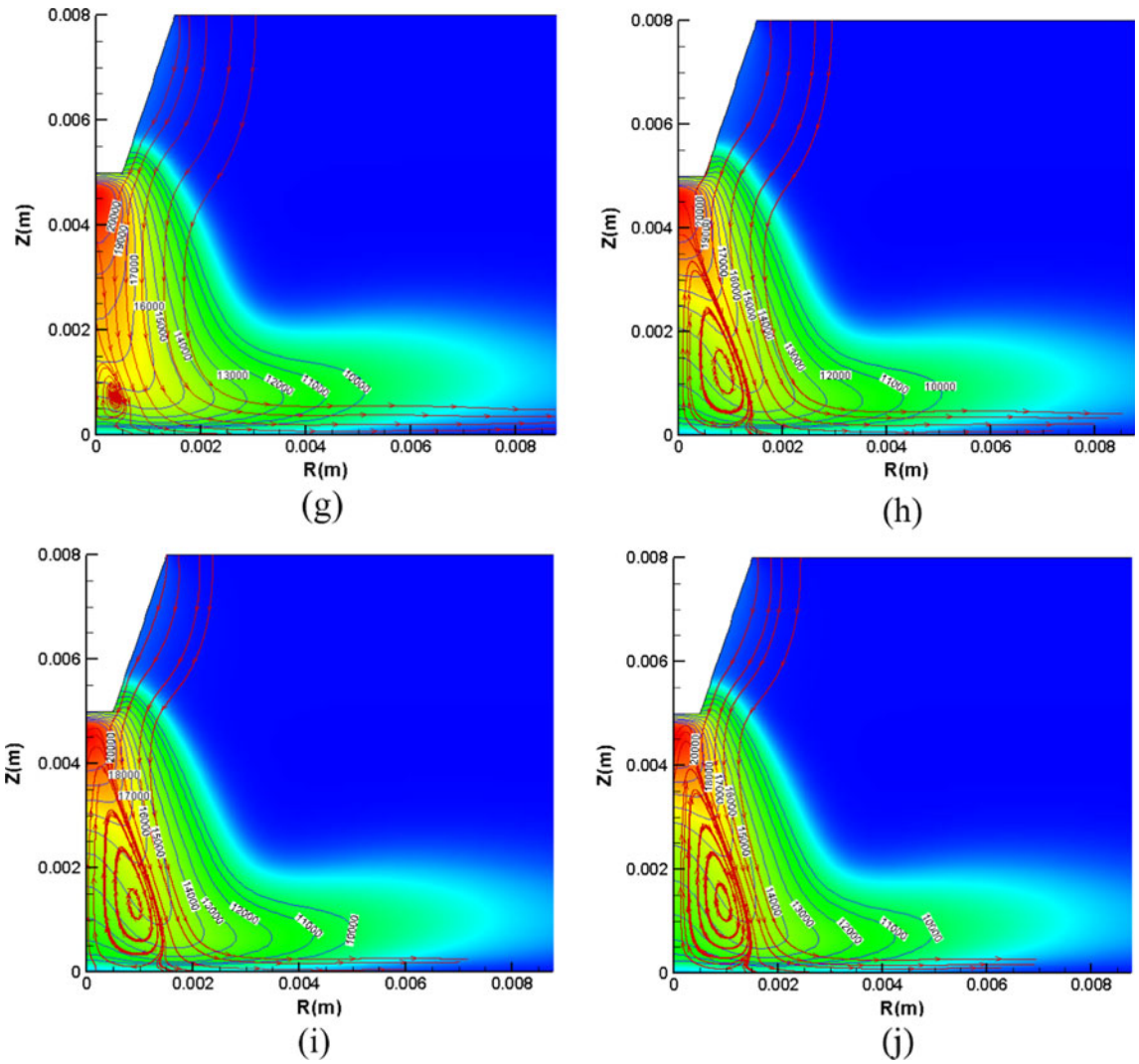

Fig. 8 (continued)

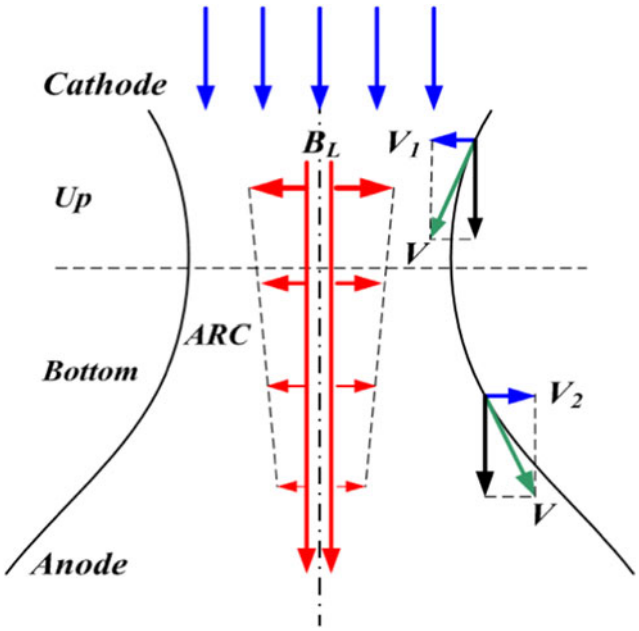

Fig. 9 The movement characteristic analyses of LMF-TIG hybrid welding arc

the radius of the particle gyrating around the symmetry axis. As a result, the gyratory radius of the particle at the upper part decreases, while the radius at the lower increases. This causes the upper part of the welding arc to contract, and the lower to expand in the macroscopic view. The upper part's contraction of the welding arc shape causes an energy concentration, which results in the increase of the peak temperature in the LMF-TIG hybrid welding (shown in Fig. 2). The temperature at the bottom near anode reduces very quickly due to the expansion of the welding arc.

At the same time, the charged particles at the arc's lower part expand under the effect of the LMF, which means the gyratory radius of the charged particles increases. In the macroscopic view, it causes an expansion in the welding arc shape (shown in Fig. 3) and a weak welding current density. The Lorentz force from the LMF is not relatively large in this condition, and hence its influence on charged particles is not obvious. With the increase of the LMF, the current density distribution transfers gradually from a single-peak shape into a bimodal one (shown in Fig. 10), and the welding arc shape changes from a solid bell shape to a hollow one. These particles are accelerated to escape from the center of the welding arc due to the effect of both LMF and arc temperature gradient. As a result, the pressure at the center of the welding arc continuously reduces in the LMF-TIG hybrid welding.

However, the effect of the Lorentz force becomes increasingly evident when the LMF induction intensity exceeds the critical value. The current density presents a bimodal distribution (shown in Fig. 10). The relatively low density of the current at the center of the welding arc indicates the low density of the charged particles. Thus, a low-temperature region is

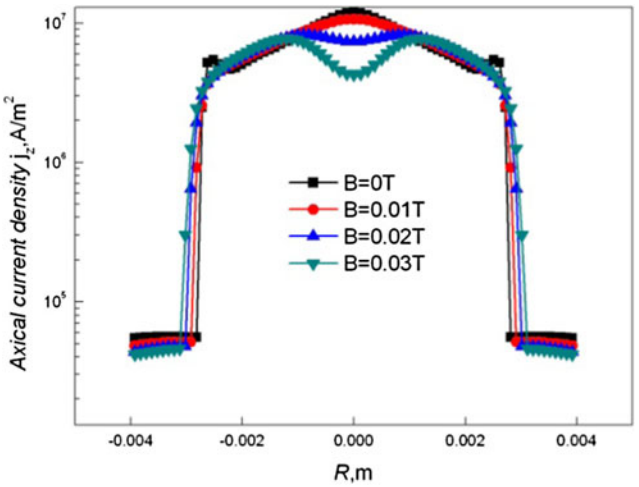

Fig. 10 Distribution of electric current density on the anode surface

formed, which is shown in Figs. 3d and 8j. At the same time, these particles escape from the center to the edge of welding arc. A lot of particles at the edge of the welding arc column are driven to take a high-speed rotation by the strong Lorentz force from the LMF. Both strong viscosity force of welding arc plasmas and centrifugal force of the rotation arc lead to the negative pressure at the center of the welding arc to appear in the LMF-TIG hybrid welding. Then, the arc plasma reversed flows and generates a suction force at the center of the welding arc. The unique suction force can be used to help the formation of welds under some special conditions, such as vertical downward welding or upward welding technology. The result in Fig. 10 agrees with other properties of the welding arc demonstrated in Figs. 6 and 8.

When keeping the LMF constant, a smaller welding current leads to a lower stiffness of the welding arc, i.e., a softer arc which is more susceptible to the interference of the LMF (shown in Fig. 4c). With the increase in the welding current, the welding arc stiffness increases resulting in a harder arc. The impact of the LMF on the welding arc reduces (shown in Fig. 5c). Thus, the expansion caused by the effect of the LMF becomes less obvious when the arc becomes harder.

4 Experiment

In order to verify the model, a water-cooled copper plate with a small hole is used to measure the pressure distribution of the welding arc on the surface of the anode. The experimental equipment is shown in Fig. 11.

The measurements for the welding arc plasmas pressure distributions are shown in Fig. 12.

The measurement and inspection system includes two parts in the Fig. 11: (1) online visual quality inspection unit and (2) real-time welding arc parameter (i.e., arc plasmas pressure and arc current density) inspection unit. The online visual quality

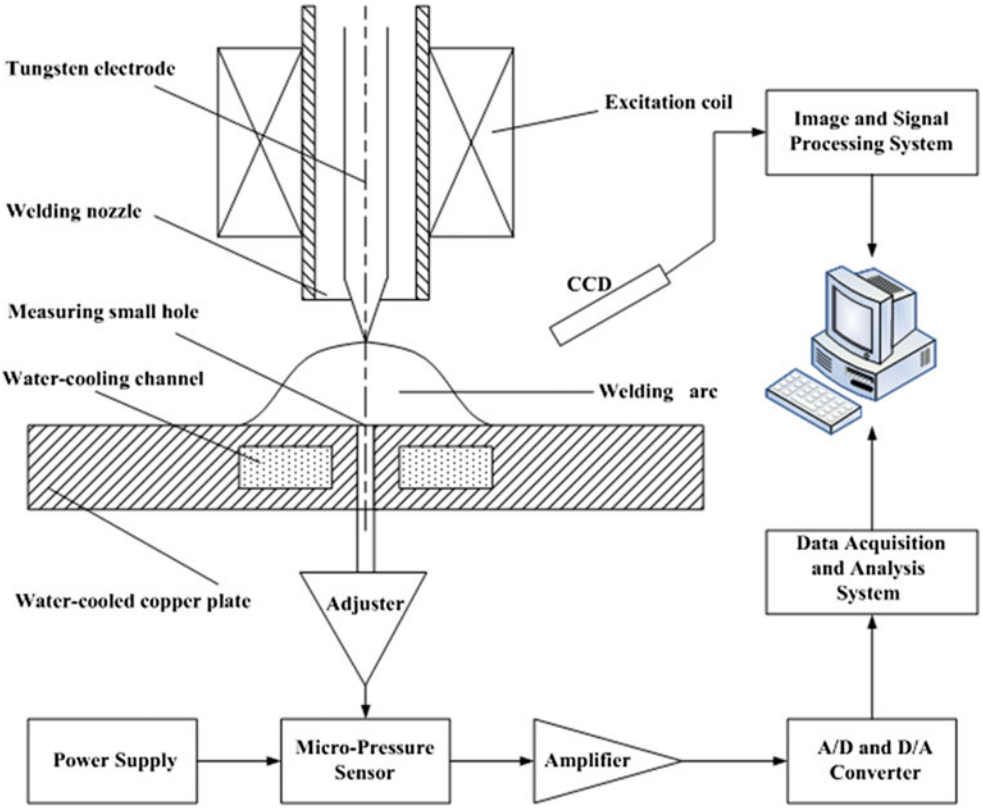

Fig. 11 Diagram of measurement device for welding arc pressure distribution

inspection part is made up of the CCD, image and signal processing system, and high-capacity computer processing system. The arc parameter inspection part composes of the water-cooling copper plate, sensor and signal processing system, and high-capacity computer processing system. There has one small hollow channel in the center of water-cooling copper plate in order to transfer the arc plasma pressure. The diameter of small hollow channel in the water-cooling copper plate is one of key factors for arc pressure measurement. In this case, the diameter of measuring small hole is less than 0.8 mm which is manufactured by a precision drilling machining method or laser processing method. The water-cooling copper plate has many inner channels with cooling water flowing. It ensures that the cooper plate cannot be fusion by the high-temperature welding arc. The LMF-TIG welding arc can be moved with a 0.1-mm sample interval distance. The sensitivity of micro-pressure sensor depended on temperature is other key to accurately measure the distribution of welding arc plasma pressure. The pressure signal is provided to high-capacity computer processing system by the A/D converter

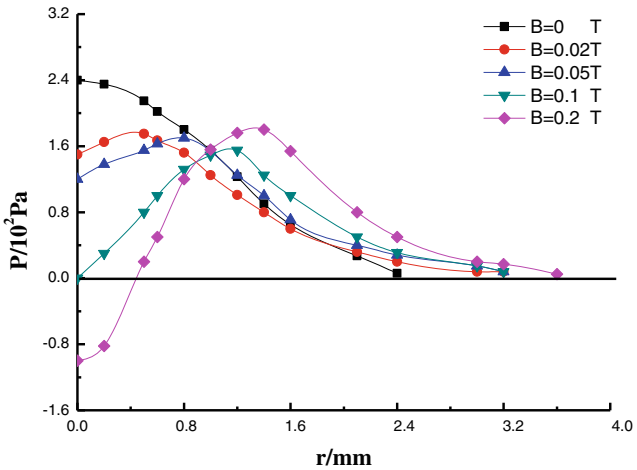

Fig. 12 Measurements and regression curves for welding arc pressure distribution

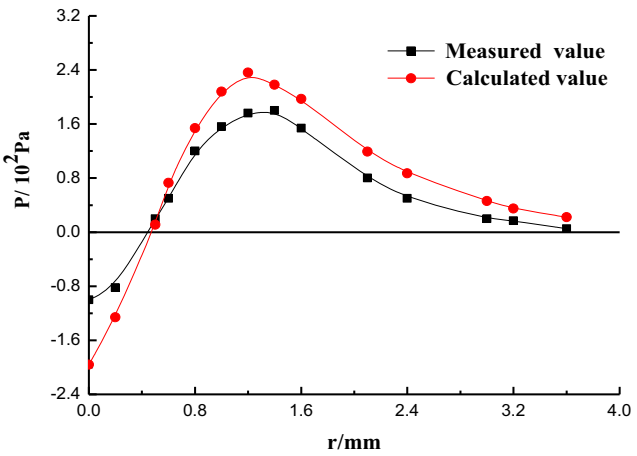

Fig. 13 Measured and calculated arc pressures on the surface of the anode. Welding current, 100 A; LMF, 0.2 T; and arc length, 3 mm

and data sample system. The sampling frequency is more that 20 KHz. In this case, the measurement experiment was taken using 100-A welding current and 3-mm length of welding arc with a weak LMF (B<0.25 T).

Figure 12 shows that the critical value of the LMF is 0.1 T when the welding current is 100 A and the arc length is 3 mm. When the LMF is greater than 0.1 T, the center of the arc exhibits a negative value. Hence, the critical value of the LMF is 0.1 T which starts to result in the formation of negative pressure at the center of the welding arc. It agrees reasonably with the model calculated critical value which is 0.08 T.

Figure 13 shows the calculated pressure distributions on the anode surface in comparison with the measurements when the LMF is 0.2 T, welding current is 100 A, and arc length is 3 mm. Reasonable agreements are observed. Based on the experiments and simulation results of welding arc (shown in the Figs. 5, 8, and 11), the welding arc is observed to look like a tornado-style behavior in the LMF-TIG hybrid welding. The unique appearance of the negative arc pressure in the LMF-TIG hybrid welding is very different from the free welding arc in typical TIG welding conditions with additional LMT. This unique phenomenon is also defined as anti-gravity gradient behavior. This kind of welding arc is called as anti-gravity gradient welding arc.

5 Conclusions

A multiphysics field numerical model has been established for the controlled arc under external longitudinal magnetic fields. The model is based on Maxwell's equations containing magnetic vector equation coupled with hydrodynamic equations. The temperature and velocity field of the welding arc were obtained. The influences of the longitudinal magnetic field strength and welding current on the welding arc were investigated.

1. The calculation results show that the temperature field and velocity field of the welding arc expand with the increase of the external longitudinal magnetic field. The increase in the magnetic field strength causes the peak temperature to rise. When the magnetic field reaches a strong strength, a low-temperature zone is formed in the center of the arc near the anode. A higher intensity of the magnetic field leads to a higher degree of expansion. With a further increase in the magnetic field strength, a circle area generates in the arc center near the anode. The maximum speed occurs on the edge of the welding arc. After that, the maximum speed reduces with the increase in the magnetic field strength.
2. According to the changes in the welding arc under different applied magnetic fields, the radial variation of the 17,000 K isotherm, φ, was defined as a standard to indicate the critical magnetic field strength (a critical value under which significant changes can take place in the electric arc). The critical value of the LMF is 0.022 T which leads to the negative pressure (i.e., anti-gravity gradient behavior) at the center of the welding arc with a 200-A welding current at 5-mm arc length. In the experimental case with 100-A current and 3-mm arc length, the negative pressure exhibits when the calculated critical value of LMF is 0.8 T, which agrees with the experimental critical value (0.1 T).
3. When the negative pressure appears below the cathode, the welding arc exhibits a tornado-style behavior with a high-speed rotation. These strong Lorentz force, viscosity force, centrifugal force, temperature gradient, and particles distribution gradient lead to the negative pressure at the center of welding arc in the LMF-TIG hybrid welding process. With the increase in the welding current, the stiffness of the welding arc increases. The welding arc becomes less susceptible to the external longitudinal magnetic field, and the trend of expansion, the temperature, and velocity field diminish. The measurement results agree with the simulation results on the same condition. The model for the welding arc in the LMF-TIG hybrid welding is thus validated by experimental data.

Acknowledgments The authors gratefully acknowledge support by the Fundamental Research Funds for the Central Universities (Project No. CDJZR13280006), Chongqing University in People's Republic of China. The authors would like to thank Prof. Dr. Zhang YM of the University of Kentucky in USA for helpful discussion.

References

1. Luo J, Wang XM, Liu D (2011) Weld pool formation and flowing behaviors of aluminum alloy during TIG welding process with a longitudinal electromagnetic field. Q J Jpn Weld Soc 29(3):71–75
2. Luo J, Luo Q, Wang X, Wang XC (2010) EMS-CO2 welding: a new approach to improve droplet transfer characteristics and welding formation. Mater Manuf Proc 25(11):1233–1241
3. Luo J, Wang X, Zhao G, Wang JX (2009) Study on mechanical properties and microstructure of gradient functional layer prepared by CO2 surfacing welding with electromagnetic stir. Acta Metall Sin 45(12):1487–1492
4. Kah P, Suoranta R, Martikainen J (2013) Advanced gas metal arc welding processes. Int J Adv Manuf Technol 67(1–4):655–674
5. Luo J, Jia CS, Wang YS, Xue J, Wu YX (2001) Mechanism of the gas tungsten-arc welding in longitudinal magnetic field controlling—I. Property of the arc. Acta Metall Sin 37(2):212–216
6. Luo J, Jia CS, Wang YS, Xue J, Wu YX (2001) Mechanism of the gas tungsten-arc welding in longitudinal magnetic field controlling—II. Model of the arc. Acta Metall Sin 37(2):217–220
7. Varghese VMJ, Suresh MR, Kumar DS (2013) Recent developments in modeling of heat transfer during TIG welding—a review. Int J Adv Manuf Technol 64(5–8):749–754
8. Farzadi A, Serajzadeh S, Kokabi AH (2008) Modeling of heat transfer and fluid flow during gas tungsten arc welding of commercial pure aluminum. Int J Adv Manuf Technol 38(3–4):258–267
9. Aval HJ, Farzadi A, Serajzadeh S, Kokabi AH (2009) Theoretical and experimental study of microstructures and weld pool geometry during GTAW of 304 stainless steel. Int J Adv Manuf Technol 42(11–12):1043–1051

10. Park JM, Kim KS, Hwang TH, Hong SH (2004) Three-dimensional modeling of arc root rotation by external magnetic field in nontransferred thermal plasma torches. IEEE Trans Plasma Sci 32(2):479–487
11. Sudhakaran R, Murugan VV, Sivasakthivel PS, Balaji M (2013) Modeling and analysis of ferrite number of stainless steel gas tungsten arc welded plates using response surface methodology. Int J Adv Manuf Technol 64(9–12):1487–1504
12. Nele L, Sarno E, Keshari A (2013) Modeling of multiple characteristics of an arc weld joint. Int J Adv Manuf Technol 69(5–8): 1331–1341
13. Balasubramanian M, Jayabalan V, Balasubramanian V (2008) A mathematical model to predict impact toughness of pulsed-current gas tungsten arc-welded titanium alloy. Int J Adv Manuf Technol 35(9–10):852–858
14. Park HJ, Kim DC, Kang MJ, Rhee S (2013) The arc phenomenon by the characteristic of EN ratio in AC pulse GMAW. Int J Adv Manuf Technol 66(5–8):867–875
15. Luo J, Xue KL, Wang C, Li LF (2013) Characteristics of light alloy/steel dissimilar metals joint by the longitudinal electromagnetic hybrid TIG welding-brazing method—II. Numerical simulation research. Q J Jpn Weld Soc 31(4):53–56
16. Zhu FL, Tsai HL, Marin SP, Wang PC (2004) A comprehensive model on the transport phenomena during gas metal arc welding process. Prog Comput Fluid Dyn 4(2):99–117
17. Kah P, Martikainen J (2013) Influence of shielding gases in the welding of metals. Int J Adv Manuf Technol 64(9–12):1411–1421
18. Fan HG, Kovacevic R (2004) A unified model of transport phenomena in gas metal arc welding including electrode, arc plasma and molten pool. J Phys D Appl Phys 37(18):2531–2544
19. Hsu KC, Etemadi K, Pfender E (1983) Study of the free-burning high-intensity argon arc. J Phys D Appl Phys 53(3):1293–1301
20. Wu CS, Ushio M, Tanaka M (1997) Analysis of the TIG welding arc behavior. Comput Mater Sci 7(3):308–314
21. Li LC, Xia WD (2008) Effect of an axial magnetic field on a DC argon arc. Chin Phys B 17(2):649–654
22. Li LC, Bai B, Zhou ZP, Xia WD (2008) Axial magnetic-field effects on an argon arc between pin and plate electrodes at atmospheric pressure. IEEE Trans Plasma Sci 36(4):1078–1079
23. Yu FL, Hu SS, Yu CL, Li L (2007) Computational simulation for the constricted flow of argon plasma arc. Comput Mater Sci 40(3): 389–394
24. Takehiko T, Tanaka J, Yasuo M, Yamatomo T, Koichi T (2005) Magnetohydrodynamic simulation of dc arc plasma under ac magnetic field. ISIJ Int 45(7):947–953
25. Tanaka M, Terasaki H, Ushio M, Lowke JJ (2002) A unified numerical modeling of stationary tungsten-inert-gas welding process. Metal Mater Trans A Phys Metal Mater Sci 33(7):2043–2052
26. Menart J, Malik S, Lin L (2000) Coupled radiative, flow and temperature-field analysis of a free-burning arc. J Phys D Appl Phys 33(3):257–269
27. Blais A, Proulx P, Boulous MI (2003) Three-dimensional numerical modelling of a magnetically deflected dc transferred arc in argon. J Phys D Appl Phys 36(5):488–496
28. Menart J, Lin L (1999) Numerical study of a free-burning argon arc with copper contamination from the anode. Plasma Chem Plasma Proc 19(2):153–170
29. Luo J, Lin X, Ye YH, Liu K (2008) Numerical study of liquid core solidification in influence of soft reduction deformation on steel slab continuous casting process. Mater Sci Forum 575–578(4): 80–85
30. Yin XQ, Gou JJ, Zhang JX, Sun JT (2012) Numerical study of arc plasmas and weld pools for GTAW with applied axial magnetic. J Phys D Appl Phys 45(28):5203–5300
31. Luo J, Luo Q, Lin YH, Xue J (2003) A new approach for fluid flow model in gas tungsten arc weld pool using longitudinal electromagnetic control. Weld J 82(8):202–206